communications physics

Article

https://doi.org/10.1038/s42005-024-01834-z

Quantum bit with telecom wave-length emission from a simple defect in Si

Peter Deák[1,2], Song Li[2] & Adam Gali[2,3,4]

Defect-related spin-to-photon interfaces in silicon promise the realization of quantum repeaters by combining advanced semiconductor and photonics technologies. Recently, controlled creation/erasure of simple carbon interstitial defects have been successfully realised in silicon. This defect has a stable structure near room temperature and coherently emits in the wave-length where the signal loss is minimal in optical fibres used in communication technologies. Our in-depth theoretical characterization confirms the assignment of the observed emission to the neutral charge state of this defect, as arising due to the recombination of a bound exciton. We also identified a metastable triplet state that could be applied as a quantum memory. Based on the analysis of the electronic structure of the defect and its similarities to a known optically detected magnetic resonance centre in silicon, we propose that a carbon interstitial can act as a quantum bit and may realize a spin-to-photon interface in complementary metal-oxide semiconductor-compatible platforms.

Silicon technology is probably the most advanced area of materials processing, and the readily available and low-cost starting materials ensure the enduring success of silicon-based electronics. Defects of the silicon crystal, which can be applied as quantum emitters and/or qubits, are receiving increasing attention recently, especially in view of integration with silicon based photonic devices. The defects suggested so far, like the G-centre (C_{Si}-I-C_{Si})[1,2], the T-centre ($[C_2]_{Si}+H$)[3,4], the W-centre (I_3)[5–7], and the C-centre (C_i+O_i)[8,9], are all complexes. (Here "I" denotes a silicon self-interstitial, the "Si" subscript a substitutional, while the "i" subscript an interstitial impurity.) The erbium-related centres[10] are even more complicated and their exact structure is not even known. Tightly controlled generation of such complexes makes defect engineering very challenging, because formation of complexes requires special annealing procedures to combine the parts of the complex, and those often lead to the formation of unwanted defects at the same time. Therefore, it would be very advantageous to find a simple defect (containing a single impurity) with the appropriate properties. Recently, a defect, with photo-luminescence (PL) in the telecom band[11,12] could have been created and erased on demand by applying femtosecond laser pulses with varying the dose of irradiation. Based on the observed spectra, the defect was identified as a single carbon interstitial (C_i)[13]. The PL of C_i is well known from earlier studies[5,14,15] and this defect has been amply characterized by deep level transient spectroscopy (DLTS)[16–18] and electron spin resonance (ESR)[18,19] as well, providing definitive information about its charge transition levels and geometrical structure. Unfortunately, to the best of our knowledge, theoretical calculations could not reproduce these properties so far[20,21], making the assignment in Ref. 13 somewhat uncertain. It is also an open question whether a single C_i defect can act as a qubit when isolated with the afore-mentioned or other techniques.

Using advanced computational techniques, in this paper we provide a full characterization of the C_i defect, in very good agreement with PL, DLTS, and ESR data, and confirm that the observed emission can really be assigned to its neutral charge state, as a radiative recombination between a bound exciton singlet state and the closed shell localized singlet state. We also find that an optically addressable metastable triplet state also exists, so the defect could be applied as a quantum memory. Comparing it to a known optical detected magnetic resonance centre in silicon (G-centre), we propose that a carbon interstitial could act as a quantum bit and may realize a spin-to-photon interface in complementary metal-oxide semiconductor-compatible platforms.

Results

The standard implementations of first-principles DFT (density functional theory) contain approximate local- or semi-local exchange functionals (LDA and GGA, respectively), which underestimate the band gap and delocalize defect states. Since defects are usually calculated in big supercells of the host crystal, the application of first-principles many-body methods are as yet computationally prohibitive. Quantitatively correct results may be obtained within (generalized) Kohn-Sham DFT by the application of semi-empirical hybrid exchange functionals, which mix semi-local and non-local (Hartee-Fock-type) exchange. We have shown earlier that the two

[1]Beijing Computational Science Research Center, Beijing, 100193, China. [2]HUN-REN Wigner Research Centre for Physics, P.O. Box 49, H-1525 Budapest, Hungary. [3]Department of Atomic Physics, Institute of Physics, Budapest University of Technology and Economics, Műegyetem rakpart 3., 1111 Budapest, Hungary. [4]MTA-WFK Lendület (Momentum) Semiconductor Nanostructures Research Group, P.O. Box 49, H-1525 Budapest, Hungary. e-mail: gali.adam@wigner.hun-ren.hu

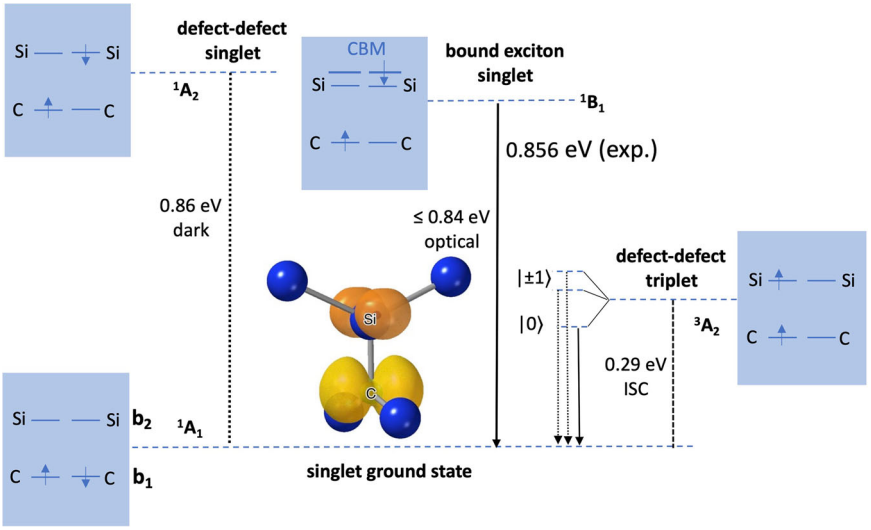

Fig. 1 | Electronic structure of C_i (alias $(C\text{-}Si)_{Si}^{[001]}$). Schematic representation of the defect states in the neutral charge state, and their occupation in the ground state and in the dark and bright singlet excited states as well as in the metastable triplet state are depicted. The zero-field splitting (ZFS) of the latter is also indicated (with $D = 439$ MHz and $E = 38$ MHz), from which intersystem crossing (ISC) may occur. The square of the wavefunction for the C 2p and the Si 3p orbital is displayed at equal isovalues. (As can be seen, the Si 3p state is less localized than the C 2p.) The wave function alternates its sign around the node. The calculated HSE06 values for the zero phonon line (ZPL) are given, but the arrows showing the transitions are not to scale. CBM denotes the conduction band minimum.

parameters of the Heyd-Scuseria-Ernzerhof (HSE) exchange functional[22], i.e., α (for mixing non-local and semi-local exchange) and μ (to describe electronic screening), can be tuned so that the functional mimics the exact DFT exchange functional[23,24]. This means that it provides the piece-wise linear behaviour of the total energy as a function of the occupation numbers, with a proper derivative discontinuity at integer values[25]. The latter is equivalent with the reproduction of the exact single-particle band gap. The linearity condition is satisfied, when the generalized Koopmans' theorem (gKT)[26] is fulfilled, i.e., the position of the highest occupied (or lowest unoccupied) Kohn-Sham level matches the ionization energy (or electron affinity), calculated from total energy differences. We have also shown that such optimized HSE(α,μ) functionals can yield very accurate results for defects in semiconductors[27–29]. Particularly in silicon, the original HSE06 = HSE(0.25,0.20) parametrization[30] is optimal, providing a (0 K) band gap of 1.16 eV, in excellent agreement with experiment[31], and resulting in charge transition levels within 0.1 eV to the measured ones[27]. Therefore, in this study, we apply the HSE(0.25,0.20) functional to calculate the properties of C_i, as described in detail in the Methods section.

As is well known from ESR signals associated with its positive charge state[18,19], the structure of the carbon interstitial, C_i, corresponds to a so-called [001] split interstitial (or dumbbell) configuration, often called $(C\text{-}Si)_{Si}^{[001]}$, with the carbon and a silicon atom sharing a lattice site, and giving rise to C_{2v} symmetry. As shown in Fig. 1, the threefold coordination results in sp^2 hybridization, with pure p-like dangling bonds on both atoms, perpendicular to each other. The C 2p dangling bond is lower in energy than the Si 3p (due to the higher electronegativity of carbon). Figure1 also shows the occupations in the neutral ground state and in the possible excited states. Removing or adding an electron preserves the C_{2v} symmetry. Table 1 shows the calculated charge transition levels in comparison to experiment. The improved agreement with respect to an earlier HSE calculation[21] may be in part due to the larger supercell, and in part due to the use of the self-consistent potential correction method, instead of an *a posteriori* energy correction (especially for the less localized negative state).

Our calculated formation energy for the neutral charge state (with respect to perfect silicon and diamond) is 3.72 eV, as also found in earlier calculations[32]. We have reported previously[33] the calculated diffusion barrier of C_i, via the reorientation mechanism of Ref. 34 to be 0.70 eV (also in good agreement with the observed values between 0.72 and 0.75 eV[18,35]), which explains the stability of this colour centre below the annealing temperature at ~50 °C[18]. (Note that the conversion of C_i to $C_{Si} + Si_i$ is endotherm by 1.86 eV so, unless mobile species are created, C_i is stable up to the temperature it begins to move.)

Table 1 | Calculated and observed charge transition levels, E(+/0) and E(0/-)

	Ref. 21	Present calculation	Experiment (at room temperature)
E(+/0)	$E_V + 0.23$ eV	$E_V + 0.32$ eV	$E_v + 0.28$ eV; Ref. 18
E(0/-)	$E_V + 0.85$ eV	$E_V + 0.97$ eV	$E_V + 1.02$ eV; Ref. 18

Note that the gap is 1.12 eV at room temperature (RT), and the acceptor level, measured to be E_C – 0.10 eV at RT, has been converted accordingly with respect to E_V. E_V and E_c are the energy of valence and conduction band edges, respectively.

Table 2 | Calculated and observed hyperfine tensor of the positively charged carbon interstitial, $^{13}C_i$

$^{13}C_i(+)$	A_{xx}(MHz)	A_{yy}(MHz)	A_{zz}(MHz)
Present calculation	12.4	12.0	169.44
Experiment; Ref. 19	18.71	17.60	145.7

We first study the ESR fingerprints of the defect which provide direct information about the localization of the defect wave functions via hyperfine interaction between the electron spin and the nuclear spins. This comparison both verifies the accuracy of our calculations and provides important information about the feasibility of employing this colour centre as a qubit. Table 2 contains the hyperfine tensor in the positive charge state, showing fair agreement with experimental values obtained on a sample enriched with ^{13}C. This indicates that the applied hybrid functional describes the localization of the defect wave functions well. Hyperfine interaction with ^{29}Si have not been published to our knowledge but we provide the calculated data in Supplementary Table 1. (We note that another ESR centre was associated with the negatively charged $(C\text{-}Si)_{Si}^{[001]}$ defect[18] but no trace of hyperfine interaction with ^{13}C or ^{29}Si – within 0.16 T ≈ 4 GHz – was found.) Based on the good agreement of the charge transition levels and the hyperfine data on the ^{13}C atom in the positive charge state, we conclude that the $(C\text{-}Si)_{Si}^{[001]}$ structure is well established, and at the same time the applied method is validated. Next, we focus on the interpretation of the PL spectrum[5,13].

The observed zero-phonon line (ZPL) associated with the C_i defect is at 0.856 eV according to the literature (see, e.g., Ref. 15), so the corresponding wave length (1448 nm) falls into the telecom region. We note that the defect is susceptible to strain (see e.g., Ref. 19) and that is likely responsible for the observed variance in the ZPL emissions of the defects in the silicon-on-insulator (SOI) sample[13] which produce a strain field towards the defects in

silicon. The observed charge transition levels clearly imply that the negative and positive charge states cannot explain this emission as they would immediately be converted to the neutral state by illumination with higher-than-ZPL energy. (If the defect was in the positive charge state then photo-excitation with higher-than-ZPL energy of the C_i center will promote an electron from the valence band to the empty defect level in the gap which turns it to neutral; if the defect was in the negative charge state then the same photo-excitation energy will promote the electron from the occupied defect level to the conduction band which again turns it to neutral.) We continue the discussion of the emission for the neutral charge state. The ground state is a closed-shell singlet which transforms as the trivial A_1. The excited state may be constructed by promoting an electron from the carbon dangling bond to the silicon dangling bond (see Fig. 1). The calculated ZPL energy (see Supplementary Note 2 for details) is 0.86 eV, including an exchange correction of 0.29 eV, which brings it close to the experimental value. However, this excited state is dark and transforms as A_2 and the optical transition is only allowed by phonon participation which clearly goes against the observed PL spectrum showing a strong ZPL emission. On the other hand, it is intriguing that the donor (+/0) charge transition level, obtained by DLTS is ≈ E_C - 0.87 eV (using the 0 K band gap for conversion where E_C is the conduction band minimum), which is only 14 meV higher than the ZPL energy. Thus, the defect may have a bound exciton excited state where the hole is located in the carbon dangling bond orbital and the electron sits on a state split from conduction band minimum (CBM) and the binding energy of the exciton is about 14 meV. Our calculations imply that the dark singlet excited state lies at higher energy than the singlet bound excited state does. Indeed, the calculated ZPL of the bound exciton recombination is 0.84 eV, in good agreement with the measured value of 0.856 eV.

By considering a singlet bound exciton state, the radiative recombination would be allowed in first order. Indeed, the calculated radiative lifetime is 2.83 μs (see Methods). The estimated radiative lifetime is relatively long because the excited state is delocalized whereas the ground state is localized, which results in a relatively weak optical transition dipole moment (0.96 D). Nevertheless, the spectrum does show a significant ZPL emission according to our simulations (see Fig. 2). The phonon sideband in the PL spectrum can be well explained by the ion relaxations going from the equilibrium geometry of the positively charged defect to that of the neutral defect. The features can be identified as the phonon modes of the Si crystal as the positively charged defect produces a larger tensile strain than the neutral one does. The calculated Huang-Rhys (HR) factor is 2.88. Based on these results, we establish the origin of the PL signal as an optical transition from a bound exciton state to the closed-shell singlet ground state of the neutral C_i defect.

We now discuss the presence of optically inactive or dark states and their roles. We assume that the dark singlet level may fall above the ionisation energy of the neutral defect. In the opposite scenario, the dark state would significantly reduce the brightness of the defect where the bright state may be activated by elevating the temperature to occupy the bright singlet state. However, it was observed in a recent study[13] that the emission intensity is decreasing with raising the temperature which clearly indicates that the dark state's level should lie above the bright state's level. The temperature dependence of the PL intensity can be explained by the thermal ionisation of the bound exciton excited state.

We have also explored a triplet manifold which is a metastable state of the defect. This may be generated by promoting an electron from the carbon dangling bond orbital to the silicon dangling bond orbital with spin flip. The corresponding $^3A_2$ level lies 0.29 eV above the ground state. The triplet state keeps the C_{2v} symmetry. The spin levels split by the orthorhombic crystal field with $D = 439.3$ MHz and $E = 37.9$ MHz. The ^{13}C and ^{29}Si hyperfine couplings are characteristic to the defect as the spin density is mostly localized on both dangling bonds (see Supplementary Table 3).

Discussion

Silicon is a very promising platform for hosting near-infrared single photon emitters and quantum bits realized by fluorescent point defects[12]. Stable

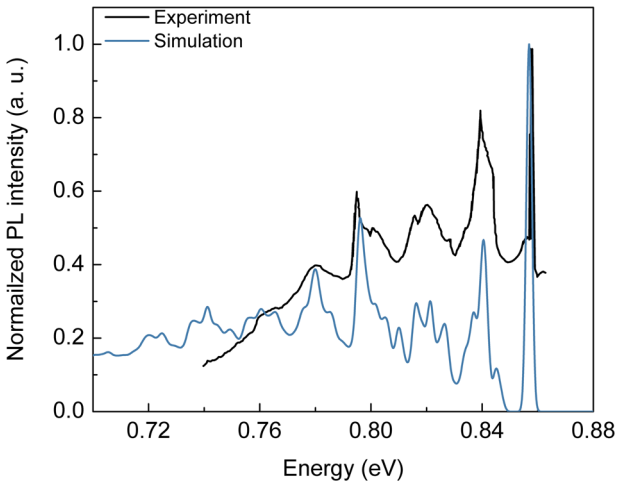

Fig. 2 | The calculated and the observed[14] photoluminescence (PL) spectra, including the phonon sidebands. Here we use the neutral and the positive charge state's geometries as ground and excited states, respectively, to generate the phonon sideband of the PL spectrum. The simulated spectrum is aligned to the experimental one at the zero-phonon line for direct comparison of the experimental and simulated phonon sidebands. We note that the experimental spectrum sits on a tail of a broad background that is not present in the simulated spectrum.

defects with a single impurity may be preferred over complexes where the latter often require difficult defect engineering protocols to create them even with relatively low yield. The recently demonstrated programmable creation of carbon interstitial defects[13] gives hope that telecom wave length single photon emitters can be generated on demand in a given density with good scalability.

The calculated radiative lifetime is 2.83 μs whereas the observed PL lifetime upon 532-nm pulsed laser excitation is between 3 and 8 ns[13]. The PL lifetime inherits both radiative and non-radiative components where various non-radiative processes may occur such as internal conversion, intersystem crossing or ionisation. Since the excitation energy of a 532-nm laser (2.33 eV) is much larger than the band gap of Si and stable positive and negative charge states of the C_i defect exist, it is likely that ionisation and re-ionisation processes occur depending on the excitation power. Indeed, the PL intensity depends non-linearly on the laser power[13] which is a clear signature that photo-ionisation processes take place in the C_i defect. Our calculated radiative rate (2.83 μs), in relation to the experimentally observed total rate (between 3 and 8 ns) implies that the quantum yield of excitation is about 0.1% at the given experimental conditions in Ref. 13 In our estimation, the Debye–Waller factor of this defect emitter is 0.056 which results in 5.6% coherent no-phonon emission of the total emission. As a consequence, observation of single defect emission requires a photonics structure at the ZPL wavelength in order to significantly enhance the PL intensity. This concept was already demonstrated for the G-centre[36] and the T-centre[37], so it is viable towards C_i emitters too. We predict that the polarization of the emitted coherent photons is perpendicular to the [001] symmetry axis based on the symmetry of the excited state and the ground state.

In order to turn the single photon emitter into a quantum repeater unit, a quantum memory should be associated with the defect. We found a metastable triplet state which can act as a quantum memory. Decay from the metastable triplet state to the singlet ground state occurs via intersystem crossing (ISC). According to group theory, the $|^3A_2, m_S = 0\rangle$ state is linked to the ground state $^1A_1$, whereas the ISC is forbidden from $|^3A_2, m_S = \pm1\rangle$ in the first order. This means that the lifetime of $|^3A_2, m_S = 0\rangle$ is shorter than that of $|^3A_2, m_S = \pm1\rangle$. This electronic structure and selection rules of ISC strongly resembles those of the G-centre in Si (Ref. 2) for which optically detected magnetic resonance (ODMR) of the electron spin was already demonstrated[38]. We provide the hyperfine coupling parameters in Supplementary Note 3 that should be assessed in future experiments for

identification of the centre. By applying a microwave pulse resonant with the $|^3A_2, m_S = 0>$ and $|^3A_2, m_S = +1>$ or $|^3A_2, m_S = -1>$ levels (see Fig. 1), a contrast in the PL emission of the C_i defect is expected upon resonant microwave transition. Proximate nuclear spins may be applied as quantum registers to store the quantum information which was encoded in the electron spin. On the other hand, too strong hyperfine interaction between the electron spin and nuclear spins has a detrimental effect on the coherence of the electron spin. According to our calculations, the hyperfine constants of ^{29}Si with $I = 1/2$ nuclear spin in the second and third neighbour shells are all in the order of 10 MHz which could significantly shorten the coherence time of the electron spin. Therefore, it is critical that the defect should be created in isotope engineered silicon with significant reduction of ^{29}Si content (to about 0.5% from the natural abundant 4.5%) so that the probability of finding one ^{29}Si around the defect up to the third neighbour shell could be reduced below 1%. The farther situated ^{29}Si nuclear spins can be safely applied as quantum memories where the quantum information from the electron spin to the nuclear spin can be realised by the Landau-Zener effect or other techniques.

Conclusion

In conclusion, our findings on the electronic structure and magneto-optical properties of a simple carbon interstitial defect in silicon establish a spin-to-photon interface with ZPL emission at the wave length compatible with the fibre optics based communication in the most mature optoelectronics platform. Our analysis revealed that it is critical to engineer this colour centre into a photonics structure for observation of single defect emission, and the ODMR experiments and quantum memory operation can be realised in ^{28}Si isotope enriched silicon host.

Methods

HSE(0.25,0.20) calculations were carried out with the Vienna ab-initio simulation package VASP 5.4, using the projector augmented wave method[39–41], and a plane wave cutoff of 420 (840) eV for the wave function (charge density). Defects were modelled in a 512-atom supercell (4×4×4 multiple of the conventional Bravais-cell), and all atoms were allowed to relax in a constant volume till the forces were below 0.01 eV/Å. The Γ-point approximation was used for Brillouin-zone sampling. The lattice constant was taken from our earlier HSE06 work[27] to be 5.4307 Å (in good agreement with experiment). Total energies of charged systems have been calculated by applying the self-consistent potential correction (SCPC) method for charge correction[42]. Charge correction was also used in the case of the bound exciton (where the electron wave function is delocalized), as described in Section 3.3.4 of Ref. 43. The zero phonon line (ZPL) was obtained as the energy difference of the relaxed ground and the relaxed excited state, the latter calculated with constrained occupation or ΔSCF method. To obtain the correct ZPL for the singlet-to-singlet transition, an exchange correction in the excited state was applied[44] in order to obtain the total energy in the spin singlet eigenstate (see also Supplementary Material in Ref. 45). In case of the bound exciton, a band-filling correction was also used[46]. (The Γ-point in the reduced Brillouin-zone of the supercell represents the [0.75,0,0] primitive k-point explicitly, while the real conduction band minimum is at [0.83,0,0]. The difference, 50 meV, was subtracted from the calculated transition energy.) The spectrum of the phonon replicas were computed by the generating function method[47], based on vibration calculations using the Perdew-Burke-Ernzerhof (PBE)[48] functional. The radiative lifetime was calculated with the inverse of $\Gamma_{\mathrm{rad}} = \frac{n_D E_{\mathrm{ZPL}}^2 \mu^2}{3\pi\varepsilon_0 c^3 \hbar^4}$ (see Ref. 49), where the optical transition dipole moment μ was calculated by taking the respective Kohn-Sham wave functions representing the electronic ground and excited states, and $n_D = 3.485$ is the refractive index of silicon at 1.45 μm or ≈0.85 eV (see Ref. 50), $E_{\mathrm{ZPL}} = 0.856$ eV is the observed energy of the ZPL, ε_0 is the dielectric permittivity of vacuum, c is the speed of light and $\hbar$ is the reduced Planck-constant.

The hyperfine tensors and zero-field splitting tensor were calculated as implemented in VASP[51,52] where the zero-field splitting tensor algorithm was implemented by Martijn Marsman.

Data availability

The authors declare that the main data supporting the findings of this study are available within the paper and its Supplementary file. Part of the source data is provided in this paper. Additional data that support the findings of this study are available from the corresponding author upon reasonable request.

Code availability

The codes that were used in this study are available upon request to the corresponding author.

Received: 19 May 2024; Accepted: 7 October 2024;
Published online: 14 October 2024

References

1. Song, L. W., Zhan, X. D., Benson, B. W. & Watkins, G. D. Bistable interstitial-carbon —substitutional-carbon pair in silicon. *Phys. Rev. B* **42**, 5765 (1990).
2. Udvarhelyi, P., Somogyi, B., Thiering, G. & Gali, A. Identification of a telecom wavelength single photon emitter in silicon. *Phys. Rev. Lett.* **127**, 196402 (2021).
3. Safonov, A. N. et al. Interstitial-carbon hydrogen interaction in silicon. *Phys. Rev. B* **77**, 4812 (1996).
4. Dhaliah, D., Xiong, Y., Sipahigil, A., Griffein, S. M. & Hautier, G. First-principles study of the T center in silicon. *Phys. Rev. Mater.* **6**, L053201 (2022).
5. Davies, G. The optical properties of luminescence centers in silicon. *Phys. Rep.* **176**, 83 (1989).
6. Tan, J., Davies, G., Hayama, S., Harding, R. & Wong-Leung, J. Ion implantation effects in silicon with high carbon content characterized by photoluminescence. *Phys. B* **340–342**, 714 (2003).
7. Baron, Y. et al. Single G centres in silicon fabricated by co-implantation with carbon and proton. *Appl. Phys. Lett.* **121**, 084003 (2022).
8. Davies, G. Carbon-related processes in crystalline silicon. *Mater. Sci. Forum* **38**, 151 (1989).
9. Udvarhelyi, P., Pershin, A., Deák, P. & Gali, A. An L-band emitter with quantum memory in silicon. *npj Comput. Mater.* **8**, 262 (2022).
10. Kenyon, A. J. Erbium in silicon. *Semicond. Sci. Technol.* **20**, R65 (2005).
11. https://www.thefoa.org/tech/ref/basic/SMbands.html
12. Zhang, G., Cheng, Y., Chou, J.-P. & Gali, A. Material platforms for defect qubits and single-photon emitters. *Appl. Phys. Rew.* **7**, 031308 (2020).
13. Jhuria, K. et al. Programmable quantum emitter formation in silicon. *Nat. Commun.* **15**, 4497 (2024).
14. Thonke, G., Teschner, A. & Sauer, R. New photoluminescence defect spectra in silicon irradiated at 100 K: Observation of interstitial carbon? *Sol. State Commun.* **61**, 241 (1987).
15. Woolley, R., Lightowlers, E. C., Tipping, A. K., Clayburn, M. & Newman, R. C. Electronic and vibrational absorption of interstitial carbon in silicon. *Mater. Sci. Forum* **10-12**, 929 (1986).
16. Lee, Y. H., Cheng, L. J., Gerson, J. D., Mooney, P. M. & Corbett, J. W. Carbon interstitial in electron-irradiated silicon. *Sol. State Commun.* **21**, 109 (1977).
17. Kimmerling, L. C., Blood, P. and Gibson, W. M. *IOP Conf. Proc. Ser.* **46**, 273 (1979).
18. Song, L. W. & Watkins, G. D. EPR identification of the single-acceptor state of interstitial carbon in silicon. *Phys. Rev. B* **42**, 5759 (1990).
19. Watkins, G. D. & Brower, K. L. EPR observation of the isolated interstitial carbon atom in silicon. *Phys. Rev. lett.* **36**, 1329 (1976).
20. Leary, P., Jones, R., Öberg, S. & Torres, V. J. B. Dynamic properties of interstitial carbon and carbon-carbon pair defects in silicon. *Phys. Rev. B* **55**, 2188 (1997).

21. Wang, H., Chroneos, A., Londos, C. A., Sgourou, E. N. & Schwingenschlögl, U. Carbon related defects in irradiated silicon revisited. *Sci. Rep.* **4**, 4909 (2014).
22. Heyd, J., Scuseria, G. E. & Ernzerhof, M. Hybrid functionals based on a screened coulomb potential. *J. Chem. Phys.* **118**, 8207 (2003).
23. Deák, P. et al. Choosing the correct hybrid for defect calculations: a case study on intrinsic carrier trapping in ß-Ga_2O_3. *Phys. Rev. B* **95**, 075208 (2017).
24. Deák, P., Lorke, M., Aradi, B. & Frauenheim, T. Optimized hybrid functionals for defect calculations in semiconductors. *J. Appl. Phys.* **126**, 130901 (2019).
25. Kaplan, A. D., Levy, M. & Perdew, J. P. The predictive power of exact constraints and appropriate norms in density functional theory. *Ann. Rev. Phys. Chem.* **74**, 193 (2023).
26. Lany, S. & Zunger, A. Polaronic hole localization and multiple hole binding of acceptors in oxide wide-gap semiconductors. *Phys. Rev. B* **80**, 085202 (2009).
27. Deák, P., Aradi, B., Frauenheim, T., Janzén, E. & Gali, A. Accurate defect levels obtained from the HSE06 range-separated hybrid functional. *Phys. Rev. B* **81**, 153203 (2010).
28. Han, M., Zeng, Z., Frauenheim, T. & Deák, P. Defect physics in intermediate-band materials: Insights from an optimized hybrid functional. *Phys. Rev. B* **96**, 165204 (2017).
29. Han, M., Deák, P., Zeng, Z. & Frauenheim, T. Possibility of Doping $CuGaSe_2$ n-Type by Hydrogen. *Phys. Rev. Appl.* **15**, 044021 (2021).
30. Krukau, A. V., Vydrov, O. A., Izmaylov, A. F. & Scuseria, G. E. Influence of the Exchange Screening Parameter on the Performance of Screened Hybrid Functionals. *J. Chem. Phys.* **125**, 224106 (2006).
31. Cardona, M. & Thewalt, M. L. Isotope effects on the optical spectra of semiconductors. *Rev. Mod. Phys.* **77**, 1174 (2005).
32. Zirkelbach, F. et al. Combined ab initio and classical potential simulation study on silicon carbide precipitation in silicon. *Phys. Rev. B* **84**, 064126 (2011).
33. Deák, P., Udvarhelyi, P., Thiering, G. & Gali, A. The kinetics of carbon pair formation in silicon prohibits reaching thermal equilibrium. *Nat. Commun.* **14**, 361 (2023).
34. Capaz, R. B., Dal Pino, A. Jr. & Joannopoulos, J. D. Identification of the migration path of interstitial carbon in silicon. *Phys. Rev. B* **50**, 7439 (1994).
35. Lastoviskii, S. et al. "Radiation-induced interstitial carbon atom in silicon: Effect of charge state on annealing characteristics" *Phys. Status Solidi A* **214**, 1700262 (2017).
36. Prabhu, M., Errando-Herranz, C., De Santis, L. & Christen, I. Cgen, Ch., Gerlach, C., and Englund, D. Individually addressable and spectrally programmable artificial atoms in silicon photonics. *Nat. Commun.* **14**, 2380 (2023).
37. Higginbottom, D. B. et al. Optical observation of single spins in silicon. *Nature* **607**, 2566 (2022).
38. O'Donnell, K. P., Lee, K. M. & Watkins, G. D. Origin of the 0.97 eV luminescence in irradiated silicon. *Phys. B* **116**, 258 (1983).
39. Kresse, G. & Hafner, J. Ab initio molecular-dynamics simulation of the liquid-metal–amorphous-semiconductor transition in germanium. *Phys. Rev. B* **49**, 14251 (1994).
40. Kresse, G. & Furthmüller, J. Efficient iterative schemes for ab initio total-energy calculations using a plane-wave basis set. *Phys. Rev. B* **54**, 11169 (1996).
41. Kresse, G. & Joubert, D. From ultrasoft pseudopotentials to the projector augmented-wave method. *Phys. Rev. B* **59**, 1758 (1999).
42. Chagas de Silva, M. et al. Self-consistent potential correction for charged periodic systems. *Phys. Rev. Lett.* **126**, 076401 (2021).
43. Gali, A. Recent advances in the ab initio theory of solid-state defect qubits. *Nanophotonics* **12**, 359 (2023).
44. Ziegler, T., Rauk, A. & Baerends, E. J. On the calculation of multiplet energies by the hartree-fock-slater method. *Theor. Chim. Acta* **43**, 261 (1977).
45. Mackoit-Sinkevičienė, M., Maciaszek, M., Van de Walle, C. G. & Alkauskas, A. Carbon dimer defect as a source of the 4.1 eV luminescence in hexagonal boron nitride. *Appl. Phys. Lett.* **115**, 212101 (2019).
46. Lany, S. & Zunger, A. Assessment of correction methods for the band-gap problem and for finite-size effects in supercell defect calculations: Case studies for ZnO and GaAs. *Phys. Rev. B* **78**, 235104 (2008).
47. Alkauskas, A., Buckley, B. B., Awschalom, D. D. & Van de Walle, C. G. First-principles theory of the luminescence lineshape for the triplet transition in diamond NV centres. *N. J. Phys.* **16**, 073026 (2014).
48. Perdew, J. P., Burke, K. & Ernzerhof, M. Generalized gradient approximation made simple. *Phys. Rev. Lett.* **77**, 3865 (1996).
49. Li, S., Thiering, G., Udvarhelyi, P., Ivády, V. & Gali, A. Carbon defect qubit in two-dimensional WS_2. *Nat. Commun.* **13**, 1210 (2022).
50. Green, M. A. Self-consistent optical parameters of intrinsic silicon at 300 K including temperature coefficients. *Sol. Energy Mater., Sol. Cells* **92**, 1305 (2008).
51. Bodrog, Z. & Gali, A. The spin–spin zero-field splitting tensor in the projector-augmented-wave method. *J. Phys. Condens. Matter* **26**, 015305 (2013).
52. Szász, K., Hornos, T., Marsman, M. & Gali, A. Hyperfine coupling of point defects in semiconductors by hybrid density functional calculations: The role of core spin polarization. *Phys. Rev. B* **88**, 075202 (2013).

Acknowledgements

A.G. acknowledges the EU HE projects QuMicro (Grant No. 101046911) and SPINUS (Grant No. 101135699). This research was supported by the Ministry of Culture and Innovation and the National Research, Development and Innovation Office within the Quantum Information National Laboratory of Hungary (Grant No. 2022-2.1.1-NL-2022-00004). We acknowledge KIFÜ for awarding us access to high-performance computation resource based in Hungary. Open access funding provided by HUN-REN Wigner Research Centre for Physics. P.D. acknowledges the support of the NSFC Grant No. 12250710132.

Author contributions

S.L. and P.D. carried out the DFT calculations under the supervision of A.G. P.D. and A.G. analysed the results. All authors contributed to the discussion and writing of the paper. A.G. conceived and led the entire scientific project.

Competing interests

The authors declare no competing interests.

Additional information

Supplementary information The online version contains supplementary material available at https://doi.org/10.1038/s42005-024-01834-z.

Correspondence and requests for materials should be addressed to Adam Gali.

Peer review information *Communications Physics* thanks Jesse Lutz and the other, anonymous, reviewer(s) for their contribution to the peer review of this work. A peer review file is available.